

Quantum optimization algorithms for CT image segmentation from X-ray data

Kyungtaek Jun*^a

^aGerman Engineering Research and Development Center, LSTME Busan Branch, Busan,

ABSTRACT

Computed tomography (CT) is an important imaging technique used in medical analysis of the internal structure of the human body. Previously, image segmentation methods were required after acquiring reconstructed CT images to obtain segmented CT images which made it susceptible to errors from both reconstruction and segmentation algorithms. However, this paper introduces a new approach using an advanced quantum optimization algorithm called quadratic unconstrained binary optimization (QUBO). This algorithm enables acquisition of segmented CT images from X-ray projection data with minimized discrepancies between experimentally obtained sinograms and quantized sinograms derived from quantized segmented CT images using the Radon transform. This study utilized D-Wave's hybrid solver system for verification on real-world X-ray data.

Keywords: Quantum segmentation, CT Image segmentation, Quantum CT Image reconstruction, Quantum annealing, QUBO, Quantum optimization algorithms

1. INTRODUCTION

The advancements in quantum computing have made quantum optimization algorithms increasingly important. Recent developments in various scientific fields^{1,2,3} have led to the creation of quadratic unconstrained binary optimization (QUBO) models specifically designed for these algorithms. The QUBO model is well-suited for utilization in gate model-based quantum computers, particularly when combined with the Quantum Approximate Optimization Algorithm (QAOA)^{4,5}. To maximize performance when working with QUBO models, it is advisable to employ a quantum annealer instead of a gate model quantum computer, as it offers superior performance compared to a gate model quantum computer. D-Wave's Advantage quantum annealer currently stands out with its impressive specifications, boasting over 5000 qubits and more than 35000 couplers. This allows for the use of 180 logical qubits with interconnections. Notably, D-Wave also offers a hybrid model that supports up to one million variables and 200 million biases.

Computed tomography (CT) is a powerful tool for non-destructive analysis of an object's internal structure, enabling detailed examination without causing any damage to the object. To obtain a segmented image from X-ray projection data, the following two steps are required. First, the CT image is reconstructed by applying the back-projection algorithm to the X-ray projection data. By applying a segmentation algorithm to the reconstructed CT image, we can obtain a segmentation image. CT employs a back-projection algorithm to reconstruct an object's internal structure based on projected images captured from different angles. An inverse projection utilizes various algorithms; iterative methods⁶, fast Fourier transform⁷, artificial intelligence⁸, and optimization^{9,10} to name a few examples. The optimization algorithm, in particular, utilizes the complete sinogram pattern to generate a more accurate image resembling the actual internal structure. By iteratively updating the sinogram using the Radon transform on a randomly generated CT image, this algorithm minimizes the disparity between the reconstructed CT image and the true sinogram. However, the computational cost associated with classical computers often hinders the quality of the obtained CT images⁹. To address this challenge, the QUBO model can be implemented on a quantum computer, leveraging its computational efficiency and resemblance to the optimization algorithm¹⁰. Nevertheless, improving CT image quality remains a hurdle within the QUBO model due to the limited number of logical qubits and the low probability of discovering the minimum energy state in a quantum computer. In the case of calculating the QUBO model for CT image reconstruction using D-Wave's hybrid solver, a solution or a good approximation was obtained even when using about 10,000 logical qubits¹¹.

*ktfriends@gmail.com

In this paper, we introduce the QUBO model for quantum segmentation that can perform both CT image reconstruction and CT image segmentation. We assume that the X-ray mass attenuation of the sample is already known. The new algorithm multiplies the X-ray mass attenuation and qubits for each pixel in the CT image. Each pixel is a quantum superposition state that can represent any value in sample and space. Afterwards, the new algorithm obtains superposed projection data by applying the same mathematical algorithm as the X-ray beam shape obtained from the X-ray projection image to the CT image in the superposed state. For each pixel, the difference between the superposed projection image and the X-ray projection image is calculated in the form of QUBO in the form of a least-squared problem. Finally, the QUBO model can be formulated by summing the QUBO form for each pixel of all projected images. We verify the new algorithm for a parallel beam X-ray light source. The size of the image used in the experiment is 50 by 50, and a total of 2,500 logical qubits were used. The mathematical projection used for superposed CT images is the Radon transform. The global minimum energy of the QUBO model was obtained using the hybrid solver of D-Wave system. We verified using a parallel beam type X-ray light source, but it is possible to use the new algorithm for any type of X-ray light source.

2. PREVIOUS RESEARCH

2.1 Radon transform and sinogram

The Radon transform mathematically describes how projection data for a parallel-beam type X-ray light source is obtained. The Radon transform can be calculated as shown:

$$R(p, \tau)[(x, y)] = \int_{-\infty}^{\infty} f(x, \tau + px) dx \quad (1)$$

$$= \int_{-\infty}^{\infty} \int_{-\infty}^{\infty} f(x, y) \delta[y - (\tau + px)] dy dx \quad (2)$$

where p is the slope of a line, τ is its intercept, and $\delta(x)$ is the delta function. A sinogram is created by accumulating Radon transforms according to angles. When using the same sample with different positions, the projected position by the Radon transform will be different. In a sinogram without motion artifacts, the shape of the projected object is said to be an ideal sinogram pattern, which is an important factor when reconstructing a CT image.

2.2 Classical optimization algorithm

Since 2017, researchers have developed an alignment method for correcting motion artifacts in the entire projection image during scanning¹²⁻¹⁵. This method, unlike previous approaches, satisfies the Helgason-Ludwig consistency condition by calculating points within the sample in a virtual space. Consequently, it enables the acquisition of high-quality CT images even when the center of rotation in space is changed. In 2021, an algorithm was introduced for reconstructing CT images based on sinogram patterns. Notably, this algorithm allows for controlling the reconstructed position of the sample within the CT image by manipulating the sinogram pattern⁹. By randomly reconstructing the CT images within a specific region of interest, the algorithm minimizes the discrepancy between the sinogram generated from the initial CT image using the Radon transform and the actual sinogram. Moreover, as it employs the complete sinogram pattern of the sample, it exhibits robustness against artifacts from specific angles. The CT image reconstruction algorithm can be mathematically formulated as an optimization problem, outlined as follows:

$$\underset{T}{\operatorname{argmin}} \text{MSE}(R(T), S) \quad (3)$$

where T is one of the CT images, S is the given sinogram, and R is the Radon transform. PyTorch (1.9.0+cu111) was used to calculate the Radon transform, and the Adam optimizer of the PyTorch library was used to calculate the optimization.

2.3 QUBO formulation for CT image reconstruction

Quantum annealers and gate model quantum computers offer the QUBO and Ising models as quantum optimization algorithms. In quantum annealing, the model's minimum value is computed, while in gate model quantum computers, the maximum value is calculated using QAOA. This paper focuses on discussing the utilization of QUBO modeling for minimization.

Typically, the pixel value in the projection image correlates with the X-ray intensity passing through the sample's thickness¹⁰. In regions where the Beer-Lambert law applies, we can express the value at the i -th position, denoted as P_i for a specific axial level, using Eq. 4.

$$P_i = \int_i^{i+1} S(x, y) dl \quad (4)$$

where $S(x, y)$ is the X-ray mass attenuation coefficient for the (x, y) -position of the sample, and the l axis is defined perpendicular to the direction of the X-ray. This equation can be expressed as a sum of discrete forms as shown in Eq. 5.

$$P_i \approx \sum a_k T_k \quad (5)$$

where a_k and T_k are the positions and proportions of pixels in the CT image that affect P_i , respectively. We may assume that T_k is the average X-ray mass attenuation coefficient for the position T_{ij} of the CT image which affects P_i . $S(i, \theta)$ is equal to P_i for the projection angle θ , as a sinogram S is an accumulation of P along the projection angle. We do not know the value of T_{ij} . In order to formulate the QUBO model, T_{ij} is expressed as the summation of qubit variables $\sum_{k=0}^m 2^k q_k^{ij}$. The QUBO model for each pixel in the sinogram is computed as follows:

$$\{(P - S)(i, \theta)\}^2 = \{\sum_k a_k T_k - S(i, \theta)\}^2 \quad (6)$$

$$= (\sum_k a_k T_k)^2 - 2S(i, \theta)(\sum_k a_k T_k) + \{S(i, \theta)\}^2 \quad (7)$$

$$= \sum_k a_k^2 T_k + 2 \sum_{i < j} a_i a_j T_i T_j - 2S(i, \theta)(\sum_k a_k T_k) + \{S(i, \theta)\}^2 \quad (8)$$

Therefore, the QUBO model for CT image reconstruction is calculated as below:

$$\sum_{\theta=0}^{180-d\theta} \sum_{i=1}^n \{(P - S)(i, \theta)\}^2 - \sum_{\theta=0}^{180-d\theta} \sum_{i=1}^n \{S(i, \theta)\}^2 \quad (9)$$

3. IMPLEMENTATION AND RESULT

3.1 Data acquisition

X-ray microcomputed tomography (μ CT) was performed at beamline 6C BioMedical Imaging o the Pohang Light Source-II¹⁶. The projection image in Fig. 1a at 2560 x 2160 pixels resolution was obtained and converted to 60 x 45 pixels resolution in Fig. 1b for experimental purposes. We did 50×50 binning around the center of rotation. Each projection image set was measured every 0.5° degrees, a total of 360 projection images per set.

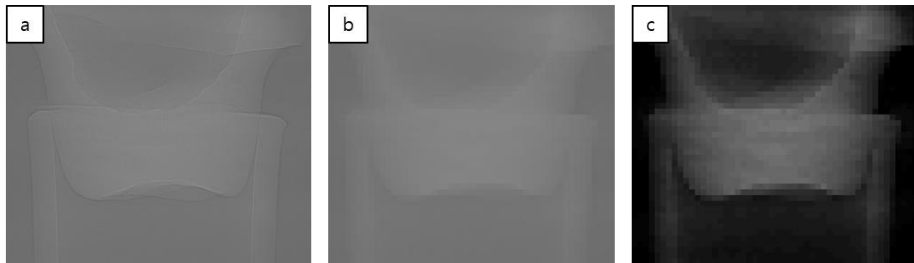


Figure 1. Acquisition and conversion of X-ray projection image. (a) Original X-ray projection image with 2560 x 2160 pixels resolution. (b) Binned X-ray projection image with 50 x 45 pixels resolution. (c) X-ray projection image with the projected area of space set to 0.

3.2 Quantum segmentation algorithm for the X-ray data

Assume that the sample exists in 3-dimensional space. Let $\alpha = \frac{\mu}{\rho}$ is X-ray mass attenuation coefficient¹⁷ and a natural number. If the number of different X-ray mass attenuation coefficients each grid space can have is m ,

then each pixel in the reconstructed image I_{ij} is represented by one of combinations of qubits and binary numbers in Eq. 10.

$$I_{ij} = \sum_{k=1}^m \alpha_k q_k^{ij} \quad (10)$$

Here, q_k^{ij} is 0 or 1, and I_{ij} have any elements of set $\{0, \alpha_1, \alpha_2, \dots, \alpha_m\}$ represents the (i, j) position in a 2-dimensional space. In three-dimensional space, use (i, j, z) instead of (i, j) where z is a axial level.

To apply optimization algorithm onto the X-ray projection data in parallel beam type, we use a Radon transform on the superposed CT image. Let IP be the superposed sinogram transformed by the CT image I . For the projection angle θ , the s -th position of IP is calculated as in Eq. 11.

$$IP(\theta, s) = c_{ij} \sum_{i,j} I'_{ij} \quad (11)$$

where I'_{ij} denotes the pixel that affects $IP(\theta, s)$ when the CT image is projected and c_{ij} is the overlapping area when I'_{ij} is projected. Applying the least square equation of the difference between $P(\theta, s)$ and $IP(\theta, s)$, the QUBO model is calculated as following:

$$(IP(\theta, s) - P(\theta, s))^2 = (c_{ij} \sum_{i,j} I'_{ij} - P(\theta, s))^2 \quad (12)$$

$$= (c_{ij} \sum_{i,j} \sum_{k=1}^m \alpha_k q_k^{ij} - P(\theta, s))^2 \quad (13)$$

$$= c_{ij}^2 \left(\sum_{i,j} \sum_{k=0}^m \alpha_k q_k^{ij} \right)^2 + 2P(\theta, s)c_{ij} \sum_{i,j} \sum_{k=1}^m \alpha_k q_k^{ij} + (P(\theta, s))^2 \quad (14)$$

In Eq. 14, the second term is linear terms in the QUBO model, and the third term represents a part of the optimization value. The first term without c_{ij}^2 is calculated as follows:

$$\left(\sum_{i,j} \sum_{k=1}^m \alpha_k q_k^{ij} \right)^2 = \sum_{i,j,k} (\alpha_k)^2 (q_k^{ij})^2 + \sum_{i \leq i', j \leq j', k \leq k'} 2\alpha_k \alpha_{k'} q_k^{ij} q_{k'}^{i'j'} \quad (15)$$

$$= \sum_{i,j,k} \alpha_k^2 q_k^{ij} + \sum_{i \leq i', j \leq j', k \leq k'} 2\alpha_k \alpha_{k'} q_k^{ij} q_{k'}^{i'j'} \quad (16)$$

To drive Eq. 16 from Eq. 15, we can convert the square terms by using $(q_k^{ij})^2 = q_k^{ij}$ because of q_k^{ij} is 0 or 1. In the second term of Eq. 16, i, j , and k cannot be equal to $i', j',$ and k' at the same time. We can calculate the first term in Eq. 14 as the sum of linear and quadratic terms as in Eq. 16.

Now we can compare two sinograms P and IP . To compute the energy minimization model, we subtract the values for each pixel in the two sinograms and square them.

$$F(\theta, s) = \sum_{\theta=0}^{180-d\theta} \sum_{s=1}^n ((IP - P)(\theta, s))^2 \quad (17)$$

where θ is the projection angle, s is the position of the sensor, and $d\theta$ is the amount of change in the projection angle. Now, $F(\theta, s)$ is expressed in linear terms, quadratic terms excluding constant terms. In the QUBO model, constant terms are excluded. The minimum value of the QUBO model is the opposite sign of the summation of constant terms.

3.3 Preprocessing of X-ray projection images

I_{ij} in Eq. 1 can take from 0 to the maximum of X-ray mass attenuation coefficient of the sample. Therefore, the sinogram of the overlapped state obtained by Radon transform also starts from 0. To express the actual X-ray projection image of the projection image made by Radon transform, a constant value must be added to I_{ij} or a constant value must be subtracted from the X-ray projection image. To express the X-ray coherence effect, more qubits must be allocated to I_{ij} . In this experiment, we will take the average of the space in the X-ray projection image and subtract it from the image (See Fig. 1c). Also, we will ignore the X-ray coherence effect. The sample is a tooth model made of resin. We made the sample out of a single material to minimize the use of logical qubits. In this case, I_{ij} can be represented as αq^{ij} .

3.4 Results

In this paper, we compare the segmented images obtained from the classical CT image and the segmentation image generated using a quantum annealer. For the classical segmented image, we generated a sinogram corresponding to the axial level indicated by the red line in Fig. 2a (See Fig. 2b). The CT image shown in Fig. 2c was reconstructed using the fast Fourier transform algorithm provided by MATLAB. Subsequently, we applied a MATLAB binarization algorithm to the CT image to identify the interior of the tooth, as depicted in Fig 2d. Finally, we obtained a segmented image of axial level 16 for the tooth sample (See Fig. 2e).

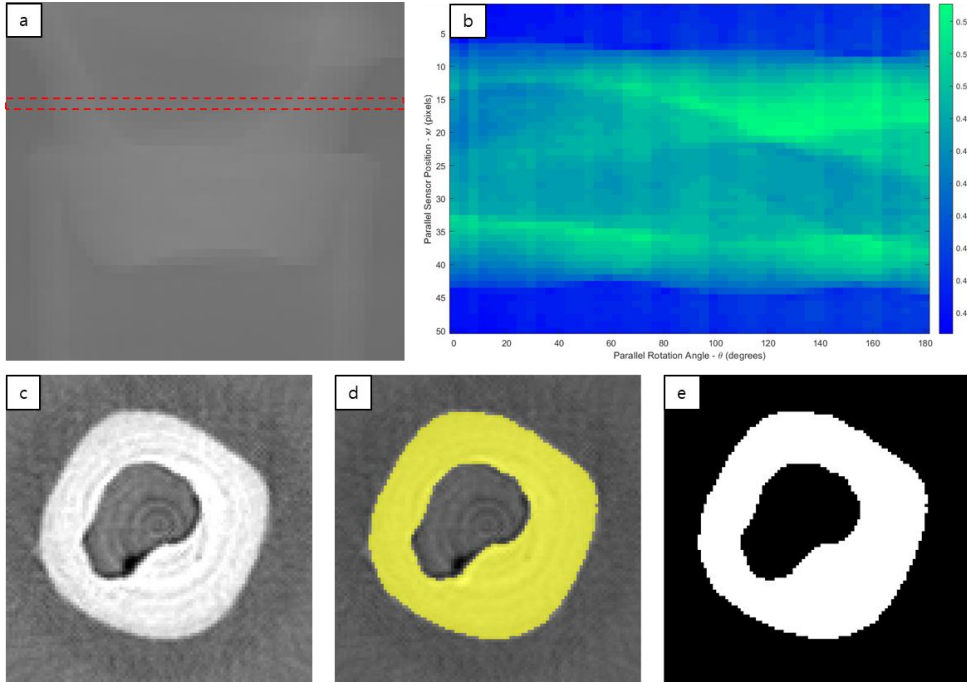


Figure 2. Classical CT image segmentation. (a) The axial level used for CT image reconstruction is displayed in red on the X-ray projection image. (b) This figure is a sinogram obtained at axial level 16. (c-e) A CT image and segmented image reconstructed by classical algorithm.

We utilize the hybrid solver of the D-Wave system to execute the quantum segmentation algorithm. This novel quantum algorithm enables the computation of segmented images directly from X-ray data in a single step. As illustrated in Fig. 3b, a sinogram is derived from the projection image, which is proportionate to the X-ray mass attenuation coefficient displayed in Fig. 3a. By formulating the QUBO model and calculating the pixel values of the sinogram using Eq. 17, we aim to represent all values through the superimposed CT image. The theoretically calculated global minimum energy is determined as the negative sum of the squared values of each pixel in the sinogram, which, in our dataset, amounts to -821370.3333333333 . Employing the solver for the QUBO model, we allocate 3 seconds to obtain 3 minimum energy values: -817517.07239 , -817516.349165 , and -817517.950592 . Figure 3c showcases the segmented image corresponding to the last energy value. Furthermore, Fig. 3d presents a comparative analysis between the segmented image derived from the classical algorithm in Fig. 2e and the segmented image obtained through the quantum optimization algorithm in Fig. 3c.

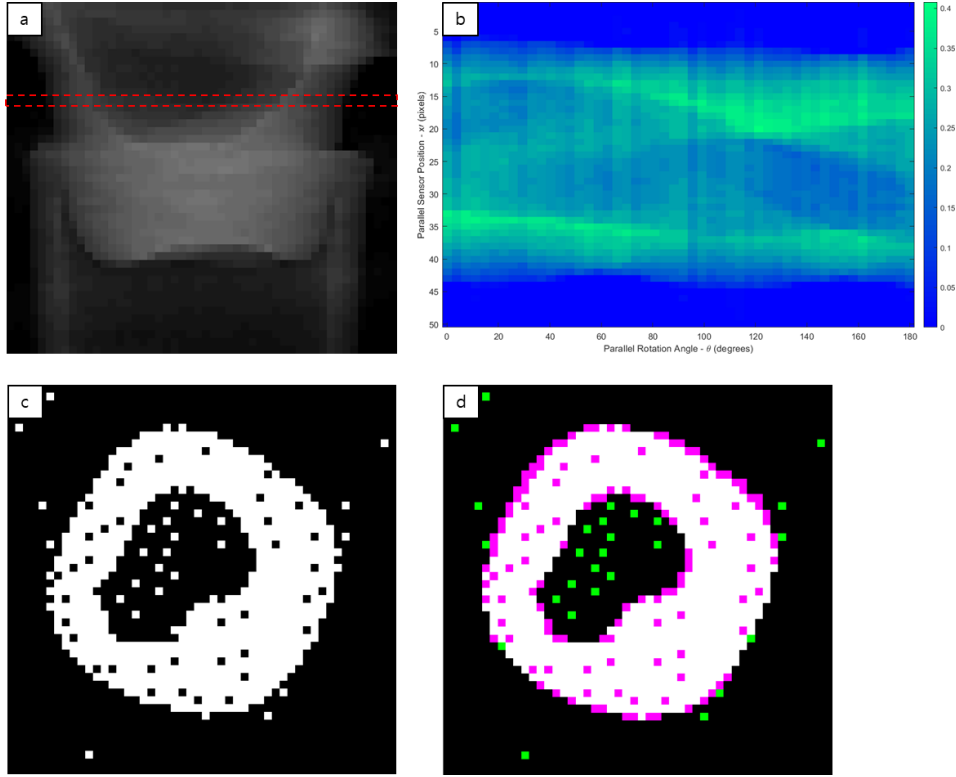


Figure 3. CT image segmentation by quantum optimization algorithm. (a) The axial level used for CT image reconstruction is displayed in red on the X-ray projection image. (b) This figure is a sinogram obtained at axial level 16. This sinogram was made proportional to the X-ray mass attenuation coefficient. (c) A segmented image by our quantum optimization algorithm. (d) This image compares two segmented images obtained by classical and quantum algorithms.

4. COUCLUSION

The quantum algorithm for CT image reconstruction¹⁰ necessitates a number of qubits equal to the number of bits in each pixel. To reconstruct a 50 by 50 CT image with a resolution of 64 bits, a total of 160,000 logical qubits are required. In contrast, the quantum segmented algorithm can reconstruct and segment the CT image with only 2,500 logical qubits, provided that the X-ray mass attenuation coefficient of the sample is known. This new algorithm enables the generation of more precise segmented CT images while using fewer logical qubits. Figure 3b represents a sinogram derived using MATLAB, which was subsequently converted to an integer value in Python. Python's sinogram values and the Radon transform applied to the segmented image in Fig. 2e were utilized to calculate the X-ray mass attenuation coefficient of the sample. For this experiment, an approximate coefficient value was employed, but we anticipate achieving more accurate results by acquiring the coefficient through experimental means. Furthermore, it is expected that better outcomes can be obtained by setting each column's value as constant in the sinogram and applying uniform normalization to the entire dataset.

Due to the utilization of the X-ray mass attenuation coefficient in the new algorithm, attaining a theoretically achievable global minimum energy is not feasible. This is because the pixels encompassing the sample's shell contain a mixture of both the sample and the surrounding space, making it impractical to represent them solely based on the X-ray mass attenuation coefficient of each pixel. However, during the segmentation process, these pixels are transformed into binary values of 0 or 1, and the new algorithm effectively addresses this issue. In this experiment, the results were calculated by running the hybrid solver of the D-Wave system three times, each for a duration of three seconds. The obtained energies differed in each iteration, and we believe that providing more

annealing time would have yielded better outcomes. Currently, we are conducting research involving samples with multiple X-ray mass attenuation coefficients, utilizing the full capacity of 1,000,000 logical qubits offered by the hybrid solver.

ACKNOWLEDGE

PBCT was conducted at beamline 6C of the Pohang Light Source-II, which is funded by the Ministry of Science and ICT (MSIT) and POSTECH in Korea. This research was supported by the quantum computing technology development program of the National Research Foundation of Korea (NRF) funded by the Korean government (Ministry of Science and ICT (MSIT)) (No. 2020M3H3A111036513).

REFERENCES

- [1] Jun, K. "QUBO formulations for system of linear equations", *arXiv preprint arXiv:2106.10819v4* (2021).
- [2] Lee, H. and Jun, K., "Range dependent Hamiltonian Algorithm for numerical QUBO formulation", *arXiv preprint arXiv:2202.07692* (2022).
- [3] Lee, H., Noh, S. and Jun, K. "Effective QUBO modeling for solving linear systems on D-wave quantum annealing device", *Quantum Information Science, Sensing, and Computation XIV*. Vol. 12093. SPIE (2022).
- [4] Farhi, E., Goldstone, J. and Gutmann, S. "A quantum approximate optimization algorithm", *arXiv preprint arXiv:1411.4028* (2014).
- [5] Zhou, L. Wang, S.-T., Choi, S., Pichler, H. and Lukin, M. D. "Quantum approximate optimization algorithm: Performance, mechanism, and implementation on near-term devices", *Physical Review X* 10.2 (2020): 021067.
- [6] Wang, X., Sabne, A., Kisner, S., Raghunathan, A., Bouman, C. and Midkiff, S. "High performance model based image reconstruction", *ACM SIGPLAN Notices* 51.8 (2016) 1-12.
- [7] Schomberg, H. and Timmer, J. "The gridding method for image reconstruction by Fourier transformation", *IEEE transactions on medical imaging* 14.3 (1995) 596-607.
- [8] Singh, R., Wu, W., Wang, G. and Kalra, M.K. "Artificial intelligence in image reconstruction: the change is here", *Physica Medica* 79 (2020) 113-125.
- [9] Kim, B.C., Lee, H. and Jun, K. "Noise-resistant reconstruction algorithm based on the sinogram pattern", *arXiv preprint arXiv:2111.10067* (2021).
- [10] Jun, K. "Highly accurate quantum optimization algorithm for CT image reconstructions based on sinogram patterns", *arXiv e-prints arXiv:-2207*.
- [11] Lee, H., Ryu, Y., Kim, J. and Jun, K. "Quantum computing for the optimization of CT image reconstruction." 2022 13th International Conference on Information and Communication Technology Convergence (ICTC). IEEE, 2022.
- [12] Jun, K. and Yoon, S. "Alignment Solution for CT Image Reconstruction using Fixed Point and Virtual Rotation Axis", *Sci. Rep.* **7**, 41218 (2017).
- [13] Jun, K. and Kim, D. "Alignment theory of parallel-beam computed tomography image reconstruction for elastic-type objects using virtual focusing method", *Plos One*, 13(6), e0198259 (2018).
- [14] Jun, K. and Jung, J. "Virtual multi-alignment theory of parallel-beam CT image reconstruction for elastic objects", *Sci. Rep.* **9** (2019) 6847.
- [15] Jun, K. "Virtual multi-alignment theory of parallel-beam CT image reconstruction for rigid objects", *Sci. Rep.* **9** (2019) 13518.
- [16] Lim, J.H., et al. "Station for structural studies on macro objects: beamline 6C Bio Medical Imaging the Pohang Light Source-II" Biodesign. Vol.5, No.2, 53-61 (2017).
- [17] Hubbell, J. H. "Photon mass attenuation and energy-absorption coefficients" *Int. J. Appl. Radiat. Isot.* 33, 1269–1290 (1982).